IEEE Access
Multidisciplinary | Rapid Review | Open Access Journal

Received May 6, 2019, accepted May 20, 2019, date of publication May 24, 2019, date of current version June 6, 2019.

Digital Object Identifier 10.1109/ACCESS.2019.2918710

Spatial Permutation Modulation for Multiple-Input Multiple-Output (MIMO) Systems

I-WEI LAI[1], (Member, IEEE), JHIH-WEI SHIH[1], CHE-WEI LEE[1], HSU-HSUAN TU[1], JUNG-CHUN CHI[2], (Student Member, IEEE), JYUN-SIAN WU[1], AND YUAN-HAO HUANG[2], (Member, IEEE)

[1]Department of Electrical Engineering, National Taiwan Normal University, Taipei 10610, Taiwan
[2]Department of Electrical Engineering, National Tsing Hua University, Hsinchu 30013, Taiwan

Corresponding author: I-Wei Lai (iweilai@ntnu.edu.tw)

This work was supported by the Ministry of Science and Technology, Taiwan, under Grant MOST 107-2221-E-003-002.

ABSTRACT Spatial modulation (SM) for the multiple-input-multiple-output (MIMO) system has attracted research interests due to its high energy and spectral efficiency. SM creates a new modulation dimension by activating a single transmit antenna according to the data bits. In this paper, we propose *spatial permutation modulation (SPM)* that modulates data bits to a *permutation vector* and activates the transmit antenna at successive time instants accordingly. The SPM achieves higher diversity and thus lower error rate since the permutation vector disperses data along the time coordinate. The theoretical model of diversity and error rate are derived in both the slow-fading channel and fast-fading channel, leading to systematic and the fast SPM design exploration. Additionally, to show that the SPM can be easily combined with other SM-based techniques, space-time block coded spatial permutation modulation (STBC-SPM) and quadrature spatial permutation modulation (QSPM) is exemplarily designed based on space-time block coded spatial modulation (STBC-SM) and quadrature spatial modulation (QSM), respectively. The numerical results demonstrate the accuracy of our theoretical analyses and the superior SPM/STBC-SPM/QSPM performances to SM/STBC-SM/QSM, respectively, especially under the severe environments like low receive diversity or spatially-correlated channel, where SM fails to provide satisfactory performance. Under the environments where systems are allowed to operate with high throughputs, SPM also achieves lower error rate performance than SM. Last but not least, inspired by SM, numerous index modulation (IM) have been invented by activating various transmission entities, e.g., subcarrier in the orthogonal frequency division multiplexing (OFDM) system. The generalization from the SM to SPM can be easily applied to another IM system for the design of index permutation modulation (IPM).

INDEX TERMS Error rate analysis, index modulation (IM), index permutation modulation (IPM), multiple-input-multiple-output (MIMO), permutation, spatial modulation (SM), spatial permutation modulation (SPM), space-time code (STC), space-time block coded spatial modulation (STBC-SM), space-time block coded spatial permutation modulation (STBC-SPM), sphere decoder, quadrature spatial modulation (QSM), quadrature spatial permutation modulation (QSPM).

I. INTRODUCTION

Multiple-input multiple-output (MIMO) technique is considered a key technology for many current wireless communication standards and the emerging 5G communication. Multiple antennas are exploited at both the transmitting and receiving ends to enhance the signal reliability and throughput, like spatial multiplexing and space–time code (STC) [1], [2]. Among various MIMO techniques, spatial modulation (SM) has gained increasing attention due to its high transmission efficiency [3]–[8].

Conventionally, the data is modulated by changing the parameters of the sinusoidal carrier wave such as the amplitude or phase. SM creates a new dimension for modulation

The associate editor coordinating the review of this manuscript and approving it for publication was Jiayi Zhang.

by exploiting the *activity status* of the transmit antennas. Specifically, SM modulates bits into two kinds of symbols: the conventional constellation symbols like quadrature amplitude modulation (QAM), and the *spatial symbols* generated by activating different transmit antennas. Taking a transmitter with 2 antennas as an example, to decide which transmit antenna is used for QAM symbol transmission, the SM modulator activates the first antenna when the spatial symbol conveys bit value '0'. Likewise, the second transmit antenna is selected when the spatial symbol conveys bit value '1'. Since different transmit antennas are used, QAM symbols are propagated through various channel fading gains. The SM receiver can thus detect the data symbols by identifying the most-likely combination of the fading gain and QAM symbol.

SM strikes a good balance among the error rate performance, throughput, and complexity. In contrast to STC and spatial multiplexing, SM only requires single radio frequency (RF) chain constituted of mixers, filters, power amplifiers, etc., resulting in huge saving of circuit complexity and power consumption. This implies that, SM can utilize the *inactive transmit antennas* to increase the throughput. Therefore, SM is considered as a competitive candidate for the 5G communications, especially in the context of the massive MIMO system [4], [7].

After SM has been proposed, the idea of *modulating data by activating different transmission antennas* has been quickly extended to various transmission entities like precoding matrices [9], transmit light emitting diodes (LEDs) for visible light communication [10], and subcarriers for the orthogonal frequency division multiplexing (OFDM) system [11], [12]. A general terminology index modulation (IM) is proposed to refer these techniques. These extensions show the value and applicability of SM for the future communications.

Nevertheless, since the spatial symbol is detected by comparing the channel fading gains of different transmit antennas, the error rate performance of SM system deteriorates in spatially-correlated channels where the *fingerprints* of the wireless channels in the spatial coordinate become similar. The other disadvantage of SM is the small transmit diversity due to the single transmitted stream, resulting in poor error rate performance if the receive antennas (receive diversity) are few [8], [13]. Several techniques like precoding or space–time shift keying (STSK) are proposed [9], [14]–[17] to gain the transmit diversity. Nevertheless, the coding matrix design is generally complicated and sometimes resort to extensive numerical simulations for optimization.

In this work, we exploit the permutation to propose a simple but yet effective technique named *spatial permutation modulation (SPM)*. Specifically, SPM disperses the spatial symbol in the time coordinate by using the permutation vector that indicates the active transmit antennas at successive time instants. Take a toy example using two transmit antennas and two time instants. In addition to the bits conveyed by the QAM symbols, the SPM transmitter modulates another bit with a permutation set $\{[1, 2]^\top, [2, 1]^\top\}$, where $(\cdot)^\top$ denotes the transpose operation. For bit '0', the permutation vector $[1, 2]^\top$ is selected, and then the first and second transmit antennas are activated at the first and second time instants, respectively. Similarly, when $[2, 1]^\top$ is selected to represent bit '1', the second and first transmit antennas are successively activated at the first and second time instants. SPM can be interpreted as a general case of SM, since the active transmit antenna index in SM is generalized to the permutation vector in SPM.

Such generalization enhances the transmission efficiency and can be easily integrated with different advanced SM techniques, e.g., space–time block coded spatial modulation (STBC-SM) [18], generalized SM (GSM) [19], [20], STSK [9], [14]–[17], and quadrature spatial modulation (QSM) [21]. To demonstrate that SPM is highly compatible with advanced SM techniques, we exemplarily design two transmission schemes integrating SPM with STBC-SM and QSM, respectively. In particular, the proposed space–time block coded spatial permutation modulation (STBC-SPM) system applies the permutation vector to select the codeword of STBC-SM at successive time instants, while the proposed quadrature spatial permutation modulation (QSPM) system utilizes two permutation vectors to convey the in-phase and quadrature signal constellations, respectively. Numerical simulations demonstrate that, by exploiting the permutations, all the SPM, STBC-SPM, and QSPM techniques achieve superior error rate performance to their counterparts, i.e., SM, STBC-SM, and QSM, respectively. It should be emphasized that the generalization from SM to SPM can be easily applied to other IM systems so as to design the index permutation modulation (IPM), which increases the impact of this work.

We analytically derive the diversity and error rate performance of SPM so as to providing theoretical understanding about the SPM system, which can be used to improve the system efficiency [22] and to optimize the transmission in a systematic way. For example, by using numerical simulations, one can discover that SPM system performs better in fast-fading channel than in slow-fading channel. Our analysis not only finds the reason behind this phenomenon, but also calculates the transmit diversity and bit error rate (BER) in both kinds of the fading channels. The analysis results reveal the design guidelines, e.g., the number of QAM repetitions should be equal to the minimum Hamming distance of permutation set so that the diversities of the QAM symbols and the permutation vectors are balanced. Moreover, the permutation has been thoroughly investigated in combinatorics, an area of discrete math [23]. Many well-known properties can be leveraged to facilitate the design of SPM [24]–[27]. Shortly summarized, the advantages of SPM are enumerated as follows:

1) **High compatibility:** SPM provides a new design direction orthogonal to most advanced SM/IM techniques, and thus can be easily integrated with them to yield a more efficient MIMO system, e.g., the proposed STBC-SPM and QSPM techniques.

2) **Systematic and fast design exploration**: The performance of SPM can be theoretically analyzed, and the fruitful research results of the permutation can be leveraged.
3) **High transmission reliability**: Because of higher transmit diversity, SPM yields better error rate performance than SM, especially under the severe environments like low receive diversity (few receive antennas) or spatially-correlated channel.
4) **Low complexity**: SPM activates one transmit antenna at a time, thus enjoying the low complexity advantage as SM, e.g., single RF chain and simple decoding algorithm.

The rest of this paper is organized as follows. Section II revisits the SM-MIMO system. Section III elaborates on the design of the SPM-MIMO transceiver. The SPM theoretical analyses including the diversity and BER are conducted in Section IV for both the slow-fading channel and fast-fading channel. STBC-SPM and QSPM are proposed in Section V as examples to show the compatibility of SPM. Section VI provides the numerical results to validate our theoretical analyses and demonstrate the superior performances of SPM, STBC-SPM, and QSPM to their counterparts, respectively. The conclusions and future works are drawn in Section VII.

II. SM-MIMO SYSTEM MODEL

We consider an $N_\mathrm{r} \times N_\mathrm{t}$ MIMO system, where N_r and N_t are the numbers of receive and transmit antennas, respectively. For the SM transmission, one transmit antenna is activated at a time so as to modulate the bits by using the QAM symbol and the index of the active transmit antenna, i.e., the spatial symbol. Let the QAM symbol $s \in \chi$ be selected from the QAM constellation set χ, the SM transmission model takes the form of

$$\mathbf{y} = \mathbf{h}_q s + \mathbf{n}, \tag{1}$$

where $\mathbf{y} \in \mathbb{C}^{N_\mathrm{r}}$ is the received signal, and $\mathbf{h}_q \in \mathbb{C}^{N_\mathrm{r}}$ is the MIMO channel vector associated with the qth transmit antenna. This activated transmit antenna index q is the spatial symbol selected by $\lfloor \log_2 N_\mathrm{t} \rfloor$ bits where $\lfloor \cdot \rfloor$ is the floor operation. Consequently, an SM symbol (s, q) conveys $\lfloor \log_2 N_\mathrm{t} \rfloor + \log_2 |\chi|$ bits, where $|\cdot|$ denotes the cardinality of the set. The additive white Gaussian noise $\mathbf{n} \in \mathbb{C}^{N_\mathrm{r}}$ is assumed to be zero mean and its covariance matrix is given by $E\left[\mathbf{n}\mathbf{n}^\mathrm{H}\right] = N_0 \mathbf{I}_{N_\mathrm{t}}$, where $E[\cdot]$ is the expectation and $\mathbf{I}_{N_\mathrm{t}}$ is an identity matrix with dimension N_t. The parameter N_0 is denoted as the noise power spectral density.

At the receiver side, the maximum likelihood (ML) detection of the SM signal is formulated as below:

$$\left(s^\star, q^\star\right) = \underset{s\in\chi, q\in[1,\ldots,N_\mathrm{t}]}{\arg\min} \left\|\mathbf{y} - \mathbf{h}_q s\right\|^2, \tag{2}$$

where $\|\cdot\|$ is the Euclidean norm. Low-complexity SM detection algorithms have been proposed, e.g., [28], [29]. Although SM is shown to be a promising communication technique, its performance is deteriorated for the case of few receive antennas or high spatial correlations [8], [13]. Consequently, we propose SPM that exploits the transmit diversity to enhance the error rate performance.

III. SPM-MIMO SYSTEM MODEL

In this section, we sequentially introduce the permutation, the way of using the permutation vectors for SPM transmission, and the SPM detection. Let $\tilde{C}_{N_\mathrm{t},T}$ be the set of *N_t-permutations of T*, i.e., all different ordered arrangements of a T-element vector of an N_t-set. For example, the permutation sets $\tilde{C}_{3,3}$ and $\tilde{C}_{3,2}$ are given by

$$\begin{aligned}\tilde{C}_{3,3} &= \left\{\begin{bmatrix}1\\2\\3\end{bmatrix}, \begin{bmatrix}1\\3\\2\end{bmatrix}, \begin{bmatrix}2\\1\\3\end{bmatrix}, \begin{bmatrix}2\\3\\1\end{bmatrix}, \begin{bmatrix}3\\1\\2\end{bmatrix}, \begin{bmatrix}3\\2\\1\end{bmatrix}\right\},\\ \tilde{C}_{3,2} &= \left\{\begin{bmatrix}1\\2\end{bmatrix}, \begin{bmatrix}1\\3\end{bmatrix}, \begin{bmatrix}2\\1\end{bmatrix}, \begin{bmatrix}2\\3\end{bmatrix}, \begin{bmatrix}3\\1\end{bmatrix}, \begin{bmatrix}3\\2\end{bmatrix}\right\}.\end{aligned} \tag{3}$$

To characterize the permutation set, we define the Hamming distance matrix $\mathbf{D}$ whose the (i, j)th entry $d_{i,j}$ represents the Hamming distance between the ith and jth permutation vectors. For example, the Hamming distance matrix of a permutation subset $\{[1, 3, 2]^\top, [2, 1, 3]^\top, [2, 3, 1]^\top, [3, 1, 2]^\top\} \subset \tilde{C}_{3,3}$ is computed as follows:

$$\mathbf{D} = \begin{bmatrix}0 & 3 & 2 & 2\\ 3 & 0 & 2 & 2\\ 2 & 2 & 0 & 3\\ 2 & 2 & 3 & 0\end{bmatrix}, \tag{4}$$

where we further define the minimum Hamming distance of a permutation set as the smallest off-diagonal component in the matrix $\mathbf{D}$, i.e.,

$$d_\mathrm{min} = \min_{i,j,\ i\neq j} d_{i,j}. \tag{5}$$

To modulate the bits by the permutation vectors, we denote the subset $C_{N_\mathrm{t},T}(K, d_\mathrm{min}) \subseteq \tilde{C}_{N_\mathrm{t},T}$ which selects K permutation vectors with the minimum Hamming distance d_min from $\tilde{C}_{N_\mathrm{t},T}$. The SPM spatial symbol is thus generated by choosing a specific permutation vector in $C_{N_\mathrm{t},T}(K, d_\mathrm{min})$ according to the data bits. Several mapping rules are investigated in [26], i.e., distance conserving mapping (DCM), distance-increasing mapping (DIM), and distance-reducing mapping (DRM). For DCM, the Hamming distances between any permutation vector pairs are equal to or larger than those of the associated encoded binary data bits. An example of a 2-bits DCM is given as follows:

$$\begin{aligned}00 &\rightarrow [1, 3, 2]^\top,\\ 01 &\rightarrow [2, 1, 3]^\top,\\ 11 &\rightarrow [2, 3, 1]^\top,\\ 10 &\rightarrow [3, 1, 2]^\top,\end{aligned} \tag{6}$$

where the associated Hamming distance matrix of these permutation vectors is provided in (4). As can be seen, the Hamming distances between arbitrary permutation pairs are equal to or larger than those of their associated binary data.

For the other mapping rules, the DIM guarantees the Hamming distances between any permutation vector pairs are larger than those of the associated binary data bits. Compared with DCM, DIM has fewer permutation vectors (K) and larger Hamming distance ($d_{\min}$). In contrast to these two mapping rules, the system using DRM has at least one permutation vector pair whose Hamming distance is less than that of the encoded binary data bits. Thus, DRM generally has highest K but smallest $d_{\min}$.

TABLE 1. Examples of permutation sets with various K and $d_{\min}$. These permutation sets are adopted in the numerical simulations of SPM, STBC-SPM, and QSPM in Section VI.

T	K	$d_{\min}$	$C_{4,T}(K, d_{\min})$
2	4	2	$[1,3]^\top, [2,4]^\top, [3,1]^\top, [4,2]^\top$
3	2	3	$[1,2,3]^\top, [2,3,4]^\top, [3,4,1]^\top, [4,1,2]^\top$
	16	1	$[1,2,3]^\top, [1,3,2]^\top, [1,4,2]^\top, [1,4,3]^\top,$ $[2,1,3]^\top, [2,1,4]^\top, [2,3,4]^\top, [2,4,1]^\top,$ $[3,1,4]^\top, [3,2,1]^\top, [3,2,4]^\top, [3,4,1]^\top,$ $[4,1,2]^\top, [4,2,3]^\top, [4,3,1]^\top, [4,3,2]^\top$
4	4	4	$[1,2,3,4]^\top, [2,3,4,1]^\top, [3,4,1,2]^\top, [4,1,2,3]^\top$
	8	3	$[1,2,3,4]^\top, [1,3,4,2]^\top, [1,4,2,3]^\top, [2,3,1,4]^\top,$ $[2,4,3,1]^\top, [2,1,4,3]^\top, [3,2,4,1]^\top, [4,1,3,2]^\top$
	16	2	$[1,2,3,4]^\top, [1,2,4,3]^\top, [1,3,2,4]^\top, [1,3,4,2]^\top,$ $[1,4,2,3]^\top, [1,4,3,2]^\top, [2,1,3,4]^\top, [2,1,4,3]^\top,$ $[2,3,1,4]^\top, [2,3,4,1]^\top, [3,1,2,4]^\top, [3,1,4,2]^\top,$ $[3,2,1,4]^\top, [3,2,4,1]^\top, [3,4,1,2]^\top, [3,4,2,1]^\top$

Table 1 lists different permutation sets. Similar to the SM spatial symbol conveying $\lfloor \log_2 N_{\mathrm{t}} \rfloor$ bits, the number of modulated bits of the SPM spatial symbol is logarithmically proportional to the size of the adopted permutation, i.e., $\lfloor \log_2 K \rfloor$. The more permutation vectors are included in $C_{N_{\mathrm{t}},T}(K, d_{\min})$, the more bits can be modulated at the expense of decreased Hamming distance. Therefore, one can flexibly adjust the parameters K and $d_{\min}$ to achieve the desired balance between the error rate performance and throughput. Note that when the transmitter is equipped with more antennas, the number of usable permutation vectors increases. The design of permutation set can be formulated as an optimization which selects K permutation vectors out of all $\frac{N_{\mathrm{t}}!}{(N_{\mathrm{t}}-T)!}$ candidates to maximize the minimum Hamming distance, where $(\cdot)!$ is the factorial operation. Although this optimization can be solved off-line and thus the computational efficiency is less significant, we propose a greedy algorithm to show that SPM is easily scalable to the systems like massive MIMO. Specifically, define all the usable permutation vectors as the candidate pool. For a permutation vector in the pool, define its neighbors as those vectors whose associated Hamming distance are shorter than $d_{\min}$. At each step of the greedy algorithm, the permutation vector with minimal number of neighbors is selected to the desired permutation set, and all its neighbors are removed from the candidate pool. If the resulting permutation set includes more than K vectors, we increase $d_{\min} = d_{\min} + 1$, denote the current permutation set as the candidate pool, and repeat the greedy algorithm again. In this way, least permutation vectors are removed from the candidate pool at each step, and the minimum Hamming distance $d_{\min}$ can be guaranteed. As demonstrated later in Sec. VI, this greedy algorithm generates satisfactory permutation set for the SPM system which performs better error rate performance than the SM system.

For the SPM transmission, according to the scenarios and user requirements, $C_{N_{\mathrm{t}},T}(K, d_{\min})$ is pre-determined and available at both the transmitter and receiver. SPM modulates $\log_2 K$ bits to a permutation vector $\mathbf{p} = [p_1, \ldots, p_T]^\top \in C_{N_{\mathrm{t}},T}(K, d_{\min})$ such that the p_tth transmit antenna is activated at the tth time instant. The received symbol vector $\mathbf{y}_t \in \mathbb{C}^{N_{\mathrm{r}}}$ is given by

$$\mathbf{y}_t = \mathbf{h}_{p_t} s_{\lceil \frac{t}{M} \rceil} + \mathbf{n}_t, \tag{7}$$

where $\mathbf{h}_{p_t}$ is the p_tth column of the channel matrix $\mathbf{H}$. The parameter M indicates the number of repetitive transmission of the QAM symbol, and $\lceil \cdot \rceil$ is the ceiling operation. This means that, for one SPM transmission, we transmit the QAM vector

$$\mathbf{s} = [\underbrace{s_1, \ldots, s_1}_{M}, \underbrace{s_2, \ldots, s_2}_{M}, \ldots, \underbrace{s_{\frac{T}{M}}, \ldots, s_{\frac{T}{M}}}_{M}]^\top. \tag{8}$$

By cascading $\mathbf{y}_t$ at different time instants $t = 1, \ldots, T$ into a received matrix $\mathbf{Y} = [\mathbf{y}_1, \ldots, \mathbf{y}_T] \in \mathbb{C}^{N_{\mathrm{r}} \times T}$, the SPM transmission model takes the form of

$$\mathbf{Y} = \mathbf{H}(\mathbf{p})\mathrm{diag}(\mathbf{s}) + \mathbf{V}, \tag{9}$$

where $\mathbf{H}(\mathbf{p}) = [\mathbf{h}_{p_1}, \ldots, \mathbf{h}_{p_T}] \in \mathbb{C}^{N_{\mathrm{r}} \times T}$ represents the *permuted channel matrix*. The matrix diag($\mathbf{s}$) is denoted as a diagonal matrix with diagonal entries being $[s_1 \ldots, s_{\frac{T}{M}}]$, and $\mathbf{V} = [\mathbf{n}_1 \ldots, \mathbf{n}_T]$ is the noise matrix.

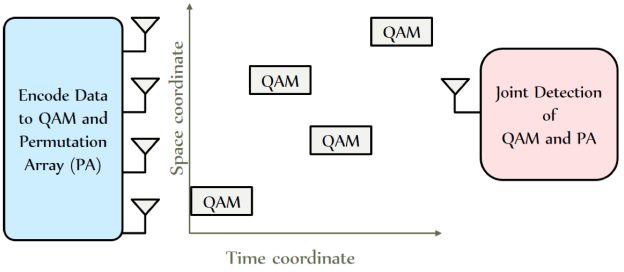

FIGURE 1. The illustration of SPM transmission with $(N_{\mathrm{t}}, N_{\mathrm{r}}, T, M) = (4, 1, 4, 4)$, i.e., the same QAM symbol is repetitively transmitted at four time instants as the system model in (10). The permutation vector $\mathbf{p} = [1, 3, 2, 4]^\top$ is used for modulation.

As mentioned previously, the trade-off between the error rate and the throughput of the spatial symbol can be adjusted by changing the permutation set $C_{N_{\mathrm{t}},T}(K, d_{\min})$. Likewise, we can design the value of M to balance the error rate and the throughput of the QAM symbol. In the extreme case of $M = T$, we have $\mathbf{s} = [s, \ldots, s]^\top$[1] so that (9) is simplified as

$$\mathbf{Y} = s\mathbf{H}(\mathbf{p}) + \mathbf{V}, \tag{10}$$

indicating that all T time instants are used to repetitively transmit the same QAM symbol as illustrated in Fig. 1

[1]For simplicity, we omit the subscript so that s_1 is represented as s.

with parameters $(N_t, N_r, T, M) = (4, 1, 4, 4)$. As can be seen, the same QAM symbol is transmitted through the first, third, second, and fourth transmit antennas at successive four time instants, respectively, according to the permutation vector $\mathbf{p} = [1, 3, 2, 4]^\top$. Since the diversity of the QAM symbol equals the number of repetitions M, the repetitive transmission reduces the error rate with the cost of lower throughput. For the opposite extreme case, we have $M = 1$ such that $\mathbf{s} = [s_1, \ldots, s_T]^\top$, that is, different QAM symbols are sent at T time instants, resulting in the highest throughput but the worst error rate performance due to the lack of the QAM diversity.

Note that based on these cases, we can interpret the SPM system with $1 < M$ as *coded SPM* using repetition code, one of the simplest coding technique. The SPM system with $M = 1$ means *uncoded SPM*. One can easily find that the SPM performance will be further improved by imposing advanced coding technique on the QAM vector $\mathbf{s}$.

For the SPM detection, the ML criterion that delivers the optimal solution $(\mathbf{s}^\star, \mathbf{p}^\star)$ can be implemented by exhaustively searching the space with $K\chi^M$ elements:

$$(\mathbf{s}^\star, \mathbf{p}^\star) = \operatorname{argmin}_{\substack{\mathbf{s}\in\chi^M,\\ \mathbf{p}\in C_{N_t,T}(K,d_{\min})}} \sum_{t=1}^{T} \|\mathbf{y}_t - \mathbf{h}_{p_t} s_{\lceil \frac{t}{M} \rceil}\|^2, \quad (11)$$

which is similar to the SM detection (2). Consequently, the low-complexity techniques invented for the SM can be extended for the efficient SPM detection. For example, we have exploited the sphere decoder to reduce the detection complexity in the preliminary SPM work [30].

The aforementioned discussion shows that SM can be considered as a special case of SPM with $T = 1$ whose permutation vector reduces to a scalar. Compared with SM, SPM inherits its low-complexity advantages with better error rate performance, especially in the cases of few receive antennas or spatially-correlated channel, which will be demonstrated later in Section VI. Nevertheless, since SPM can flexibly adjust its parameters to achieve various trade-offs between the error rate performance and throughput, its performance optimization is time-consuming if resorting to the numerical Monte Carlo simulations. In the following section, we show that the SPM performance can be theoretically analyzed, which provides systematic and fast design exploration.

IV. THEORETICAL DIVERSITY AND ERROR RATE ANALYSIS OF SPM

In this section, we analyze the diversity and the error rate performance of SPM in both slow-fading channel and fast-fading channel, starting with the pair-wise error probability (PEP)

$$f(\mathbf{s}, \mathbf{p} \to, \tilde{s}, \tilde{\mathbf{p}}) \triangleq P(\Lambda(\mathbf{s}, \mathbf{p}, \tilde{s}, \tilde{\mathbf{p}}) < 0), \quad (12)$$

which represents the probability that given the transmitted signals $(\mathbf{s}, \mathbf{p})$, the receiver discovers that $(\tilde{\mathbf{s}}, \tilde{\mathbf{p}})$ has a larger likelihood. $\Lambda(\mathbf{s}, \mathbf{p}, \tilde{\mathbf{s}}, \tilde{\mathbf{p}})$ is the log-likelihood ratio (LLR) of $P(\mathbf{Y}|\mathbf{s}, \mathbf{p}, \mathbf{H})$ to $P(\mathbf{Y}|\tilde{\mathbf{s}}, \tilde{\mathbf{p}}, \mathbf{H})$:

$$\Lambda(\mathbf{s},\mathbf{p},\tilde{\mathbf{s}},\tilde{\mathbf{p}}) \triangleq \log P(\mathbf{Y}|\mathbf{s}, \mathbf{p}, \mathbf{H}) - \log P(\mathbf{Y}|\tilde{\mathbf{s}}, \tilde{\mathbf{p}}, \mathbf{H}). \quad (13)$$

Due to the AWGN assumption, $P(\mathbf{Y}|\mathbf{s}, \mathbf{p}, \mathbf{H})$ can be written as

$$P(\mathbf{Y}|\mathbf{s}, \mathbf{p}, \mathbf{H}) = (N_0\pi)^{-TN_r} \prod_{t=1}^{T} e^{-\frac{\|\mathbf{y}_t - \mathbf{h}_{p_t} s_{\lceil \frac{t}{M} \rceil}\|^2}{N_0}}. \quad (14)$$

By inserting (14) to (13), we have

$$\Lambda(\mathbf{s},\mathbf{p},\tilde{\mathbf{s}},\tilde{\mathbf{p}}) = \sum_{t=1}^{T} \frac{\|\mathbf{h}_{p_t} s_{\lceil \frac{t}{M} \rceil} - \mathbf{h}_{\tilde{p}_t} \tilde{s}_{\lceil \frac{t}{M} \rceil}\|^2 + 2\,\mathrm{Re}\left\{(\mathbf{h}_{p_t} s_{\lceil \frac{t}{M} \rceil} - \mathbf{h}_{\tilde{p}_t} \tilde{s}_{\lceil \frac{t}{M} \rceil})^{\mathrm{H}} \mathbf{n}_t\right\}}{N_0}, \quad (15)$$

where $(\cdot)^{\mathrm{H}}$ is the Hermitian operation and $\mathrm{Re}\{\cdot\}$ is the real part. Conditioned on $\mathbf{H}$, Λ is a Gaussian random variable whose mean $\bar{\Lambda}$ takes the forms of

$$\bar{\Lambda} = \sum_{t=1}^{T} \mu_t \quad (16)$$

with

$$\mu_t = \frac{1}{N_0} \|\mathbf{h}_{p_t} s_{\lceil \frac{t}{M} \rceil} - \mathbf{h}_{\tilde{p}_t} \tilde{s}_{\lceil \frac{t}{M} \rceil}\|^2. \quad (17)$$

The variance of Λ is derived accordingly

$$\sigma_\Lambda^2 = 2\bar{\Lambda} = 2\sum_{t=1}^{T} \mu_t. \quad (18)$$

Now, we are able to derive the conditional moment-generating function (MGF) of the Gaussian random variable Λ

$$M_\Lambda(z|\mathbf{H}) = e^{(z+z^2)\bar{\Lambda}} = \prod_{t=1}^{T} e^{(z+z^2)\mu_t}. \quad (19)$$

To further remove the channel conditions, we have to characterize the distribution of μ_t in slow-fading channel and fast-fading channel, respectively.

A. DISTRIBUTION OF μ_T IN SLOW-FADING CHANNEL

The distribution of μ_t depends on the relationship between p_t and $\tilde{p}_t$. When $p_t = \tilde{p}_t$, μ_t in (17) can be simplified to

$$\mu_t = \frac{1}{N_0} \|\mathbf{h}_{p_t}\|^2 |s_{\lceil \frac{t}{M} \rceil} - \tilde{s}_{\lceil \frac{t}{M} \rceil}|^2, \quad p_t = \tilde{p}_t, \quad (20)$$

which is a Gamma distribution Γ with the shape parameter N_r and the scale parameter $\frac{\sigma_h^2}{N_0}(|s_{\lceil \frac{t}{M} \rceil} - \tilde{s}_{\lceil \frac{t}{M} \rceil}|^2)$. The random variables μ_{t_1} and μ_{t_2} for $t_1 \neq t_2$ are independent, since $h_{p_{t_1}}$ and $h_{p_{t_2}}$ are the channel gains associated with the p_{t_1}th and the p_{t_2}th transmit antennas, respectively.

Nevertheless, when $p_t \neq \tilde{p}_t$, μ_{t_1} and μ_{t_2} for $t_1 \neq t_2$ may be dependent since they may comprise the same channel fading

gains. Taking $\mathbf{p} = [1, 2, 3, 4]^\top$ and $\tilde{\mathbf{p}} = [1, 2, 4, 3]^\top$ as an example, we have dependent μ_3 and μ_4 at the third and fourth time instants

$$\mu_3 = \frac{1}{N_0}\|\mathbf{h}_3 s_{\lceil \frac{3}{M} \rceil} - \mathbf{h}_4 \tilde{s}_{\lceil \frac{3}{M} \rceil}\|^2,$$
$$\mu_4 = \frac{1}{N_0}\|\mathbf{h}_4 s_{\lceil \frac{4}{M} \rceil} - \mathbf{h}_3 \tilde{s}_{\lceil \frac{4}{M} \rceil}\|^2, \tag{21}$$

since they are both the functions of $\mathbf{h}_3$ and $\mathbf{h}_4$.

Consequently, when taking the expectation over $\mathbf{H}$ to remove the channel condition in (19) for the slow-fading channel, we have

$$M_\Lambda(z) = E_{\mathbf{H}}\{M_\Lambda(z|\mathbf{H})\} = E_{\mathbf{H}}\left\{\prod_{t=1}^{T} e^{(z+z^2)\mu_t}\right\}$$
$$= \prod_{\substack{t \\ p_t=\tilde{p}_t}} E_{\mathbf{H}}\left\{e^{(z+z^2)\mu_t}\right\} E_{\mathbf{H}}\left\{\prod_{\substack{t \\ p_t\neq\tilde{p}_t}} e^{(z+z^2)\mu_t}\right\}, \tag{22}$$

where the last equation factorizes the MGF into two product sequences in the right-hand side (RHS), because $(\mathbf{h}_{p_t}, \mathbf{h}_{\tilde{p}_t})$ for $p_t = \tilde{p}_t$ and $p_t \neq \tilde{p}_t$ are associated with different transmit antennas and thus independent. Due to the *time dependency* explained previously, the expectation of the second product series ($p_t \neq \tilde{p}_t$) cannot be directly computed by individually taking the expectation of each $e^{(z+z^2)\mu_t}$ and computing their product. Nevertheless, we have observed the empirical distribution of the term $\sum_{\substack{t \\ p_t\neq\tilde{p}_t}} \mu_t$ and used Gamma distribution for approximation

$$\sum_{\substack{t \\ p_t\neq\tilde{p}_t}} \mu_t \sim \Gamma(k, \theta), \tag{23}$$

where (k, θ) is obtained by resorting to the machine learning algorithm. In particular, the full connected neural network was adopted with the activation function *tanh*, back propagation algorithm and least square objective function to learn (k, θ) through the empirical distributions [31]. With this approximation, (22) is computed as follows:

$$M_\Lambda(z) = \prod_{\substack{t \\ p_t=\tilde{p}_t}} \left(1 - \frac{\sigma_h^2}{N_0}|s_{\lceil \frac{t}{M} \rceil} - \tilde{s}_{\lceil \frac{t}{M} \rceil}|^2(z^2+z)\right)^{-N_\mathrm{r}} \left(1 - \theta(z^2+z)\right)^{-kN_\mathrm{r}}. \tag{24}$$

B. DISTRIBUTION OF μ_T IN FAST-FADING CHANNEL

In fast-fading channel, since the fading gain varies over time, μ_{t_1} and μ_{t_2} are independent random variables for $t_1 \neq t_2$, regardless of the relationship between p_t and $\tilde{p}_t$. Therefore, once the distribution of μ_t is known, the unconditional MGF $M_\Lambda(z)$ can be computed easily. Similar to the case in slow-fading channel, μ_t is a Gamma random variable when $p_t = \tilde{p}_t$ by observing the formulation (20).

When $p_t \neq \tilde{p}_t$, the random variable μ_t is the summation of N_r independent and identically distributed (i.i.d.) squared norms, i.e., $|h_{r,p_t} s_{\lceil \frac{t}{M} \rceil} - h_{r,\tilde{p}_t} \tilde{s}_{\lceil \frac{t}{M} \rceil}|^2$ for $r = 1, \ldots, N_\mathrm{r}$. Since both h_{r,p_t} and $h_{r,\tilde{p}_t}$ are complex Gaussian random variables, the magnitude of their summation $|h_{r,p_t} s_{\lceil \frac{t}{M} \rceil} - h_{r,\tilde{p}_t} \tilde{s}_{\lceil \frac{t}{M} \rceil}|$ is a Rayleigh random variable

$$|h_{r,p_t} s_{\lceil \frac{t}{M} \rceil} - h_{r,\tilde{p}_t} \tilde{s}_{\lceil \frac{t}{M} \rceil}| \sim \mathcal{R}(\sigma_h \sqrt{|s_{\lceil \frac{t}{M} \rceil}|^2 + |\tilde{s}_{\lceil \frac{t}{M} \rceil}|^2}). \tag{25}$$

Constituted by the summation of N_r i.i.d. squared Rayleigh random variables, μ_t is a Gamma random variable for $p_t \neq \tilde{p}_t$ as well. Therefore, the Gamma random variable μ_t can be represented with different scale parameters depending on the relationship between p_t and $\tilde{p}_t$:

$$\mu_t \sim \begin{cases} \Gamma(N_\mathrm{r}, \frac{\sigma_h^2}{N_0}(|s_{\lceil \frac{t}{M} \rceil} - \tilde{s}_{\lceil \frac{t}{M} \rceil}|^2)), & p_t = \tilde{p}_t \\ \Gamma(N_\mathrm{r}, \frac{\sigma_h^2}{N_0}(|s_{\lceil \frac{t}{M} \rceil}|^2 + |\tilde{s}_{\lceil \frac{t}{M} \rceil}|^2)), & p_t \neq \tilde{p}_t \end{cases}. \tag{26}$$

By using this result and (19), the channel conditions of the MGF of Λ is removed

$$M_\Lambda(z) = \prod_{t=1}^{T} \left(1 - \frac{\sigma_h^2}{N_0}\beta_t(z^2+z)\right)^{-N_\mathrm{r}}, \tag{27}$$

with

$$\beta_t = \begin{cases} |s_{\lceil \frac{t}{M} \rceil} - \tilde{s}_{\lceil \frac{t}{M} \rceil}|^2, & \text{if } p_t = \tilde{p}_t, \\ |s_{\lceil \frac{t}{M} \rceil}|^2 + |\tilde{s}_{\lceil \frac{t}{M} \rceil}|^2, & \text{if } p_t \neq \tilde{p}_t. \end{cases} \tag{28}$$

C. DIVERSITY AND BER CALCULATION

It is known that the diversity λ determines the speed of the error rate performance improvement as the signal-to-noise ratio (SNR) increases with the definition of

$$\lambda(\mathbf{s}, \mathbf{p} \to \tilde{\mathbf{s}}, \tilde{\mathbf{p}}) = -\lim_{\frac{\sigma_h^2\sigma_s^2}{N_0}\to\infty} \frac{\log f(\mathbf{s}, \mathbf{p} \to \tilde{\mathbf{s}}, \tilde{\mathbf{p}})}{\log \frac{\sigma_h^2\sigma_s^2}{N_0}}, \tag{29}$$

where σ_s^2 is the signal power. To analyze the diversity, we apply the Chernoff bound of the PEP by using $M_\Lambda(z)$:

$$f_{\mathrm{CB}}(\mathbf{s}, \mathbf{p} \to \tilde{\mathbf{s}}, \tilde{\mathbf{p}}) = M_\lambda(\hat{z}), \tag{30}$$

where $\hat{z} = \frac{1}{2}$ by calculating $(logM_\Lambda(\hat{z}))' = 0$. Let $f_{\mathrm{CB,s}}(\mathbf{s}, \mathbf{p} \to \tilde{\mathbf{s}}, \tilde{\mathbf{p}})$ and $f_{\mathrm{CB,f}}(\mathbf{s}, \mathbf{p} \to \tilde{\mathbf{s}}, \tilde{\mathbf{p}})$ be the PEP bound in slow-fading channel and fast-fading channel, respectively. By using the results in (24) and (27), we have

$$f_{\mathrm{CB,s}}(\mathbf{s}, \mathbf{p} \to \tilde{\mathbf{s}}, \tilde{\mathbf{p}}) = \left(\prod_{\substack{t \\ p_t=\tilde{p}_t}} \left(1 + \frac{\sigma_h^2}{4N_0}|s_{\lceil \frac{t}{M} \rceil} - \tilde{s}_{\lceil \frac{t}{M} \rceil}|^2\right)^{-N_\mathrm{r}}\right)\left(1 + \frac{\sigma_h^2}{4N_0}\theta\right)^{-kN_\mathrm{r}} \tag{31}$$

and

$$f_{\mathrm{CB,f}}(\mathbf{s}, \mathbf{p} \to \tilde{\mathbf{s}}, \tilde{\mathbf{p}}) = \prod_{t=1}^{T} \left(1 + \frac{\sigma_h^2}{4N_0}\beta_t\right)^{-N_\mathrm{r}}. \tag{32}$$

Inserting these Chernoff bounds to (29), the diversity in slow-fading channel can be computed

$$\lambda_s(\mathbf{s},\mathbf{p}\to\tilde{\mathbf{s}},\tilde{\mathbf{p}}) = -\lim_{\frac{\sigma_h^2\sigma_s^2}{N_0}\to\infty} \frac{\left(\prod_{tp_t=\tilde{p}_t}\left(1+\frac{\sigma_h^2}{4N_0}|s_{\lceil\frac{t}{M}\rceil}-\tilde{s}_{\lceil\frac{t}{M}\rceil}|^2\right)^{-N_r}\right)\left(1+\frac{\sigma_h^2}{4N_0}\theta\right)^{-kN_r}}{\log\frac{\sigma_h^2\sigma_s^2}{N_0}}$$

$$= N_r \lim_{\frac{\sigma_h^2\sigma_s^2}{N_0}\to\infty} \frac{\log\sum_{tp_t=\tilde{p}_t}\left(1+\frac{\sigma_h^2}{4N_0}|s_{\lceil\frac{t}{M}\rceil}-\tilde{s}_{\lceil\frac{t}{M}\rceil}|^2\right)}{\log\frac{\sigma_h^2\sigma_s^2}{N_0}} + kN_r \lim_{\frac{\sigma_h^2\sigma_s^2}{N_0}\to\infty} \frac{\log\left(1+\frac{\sigma_h^2}{4N_0}\theta\right)}{\log\frac{\sigma_h^2\sigma_s^2}{N_0}}$$

$$\overset{(a)}{=} \Big(\sum_{\substack{t\\ p_t=\tilde{p}_t}} \mathbf{1}_{s_{\lceil\frac{t}{M}\rceil}\neq\tilde{s}_{\lceil\frac{t}{M}\rceil}} + k\Big)N_r, \tag{33}$$

where $\mathbf{1}_{s_{\lceil\frac{t}{M}\rceil}\neq\tilde{s}_{\lceil\frac{t}{M}\rceil}}$ is the indicator function that outputs 1 when $s_{\lceil\frac{t}{M}\rceil}\neq\tilde{s}_{\lceil\frac{t}{M}\rceil}$ and 0 otherwise. The equality (a) is due to the fact that

$$\lim_{x\to\infty}\frac{\log(1+ax)}{\log x} = \lim_{x\to\infty}\frac{\log(ax)}{\log x} = \lim_{x\to\infty}\frac{\log a+\log x}{\log x} = 1 \tag{34}$$

Likewise, the diversity in fast-fading channel is calculated as follows:

$$\lambda_f(\mathbf{s},\mathbf{p}\to\tilde{\mathbf{s}},\tilde{\mathbf{p}})0$$

$$= -\lim_{\frac{\sigma_h^2\sigma_s^2}{N_0}\to\infty} \frac{\left(1+\frac{\sigma_h^2}{4N_0}\beta_t\right)^{-N_r}}{\log\frac{\sigma_h^2\sigma_s^2}{N_0}}$$

$$= N_r \lim_{\frac{\sigma_h^2\sigma_s^2}{N_0}\to\infty} \frac{\sum_{p_t=\tilde{p}_t}\left(1+\frac{1}{4N_0}\sigma_h^2|s_{\lceil\frac{t}{M}\rceil}-\tilde{s}_{\lceil\frac{t}{M}\rceil}|^2\right)}{\log\frac{\sigma_h^2\sigma_s^2}{N_0}} + N_r \lim_{\frac{\sigma_h^2\sigma_s^2}{N_0}\to\infty} \frac{\sum_{p_t\neq\tilde{p}_t}\left(1+\frac{1}{4N_0}\sigma_h^2\left(|s_{\lceil\frac{t}{M}\rceil}|^2+|\tilde{s}_{\lceil\frac{t}{M}\rceil}|^2\right)\right)}{\log\frac{\sigma_h^2\sigma_s^2}{N_0}}$$

$$= \Big(\sum_{\substack{t\\ p_t=\tilde{p}_t}} \mathbf{1}_{s_{\lceil\frac{t}{M}\rceil}\neq\tilde{s}_{\lceil\frac{t}{M}\rceil}} + d(\mathbf{p},\tilde{\mathbf{p}})\Big)N_r$$

$$\overset{(a)}{\geq} \Big(\sum_{\substack{t\\ p_t=\tilde{p}_t}} \mathbf{1}_{s_{\lceil\frac{t}{M}\rceil}\neq\tilde{s}_{\lceil\frac{t}{M}\rceil}} + d_{\min}\Big)N_r, \tag{35}$$

where $d(\mathbf{p},\tilde{\mathbf{p}}) \geq d_{\min}$ is the Hamming distance between the permutation vector $\mathbf{p}$ and $\tilde{\mathbf{p}}$. Such Hamming distance equals the number of time instants with $p_t \neq \tilde{p}_t$. Considering the system transmitting single QAM symbol ($M = T$), the PEP with $s \neq \tilde{s}$ shows that its QAM diversity can be up to TN_r in fast-fading channel, since all the $T - d_{\min}$ indicator functions equal 1. Thus, when $M \leq T$, the diversity of each QAM symbol is MN_r, independent to the permutation.

Meanwhile, the diversity of the spatial symbol is computed by considering the error pairs with $\mathbf{s} = \tilde{\mathbf{s}}$, which equals kN_r and $d_{\min}N_r$ in slow-fading channel and fast-fading channel, respectively. With the diversity analyses, we can have the systematic and fast design of the SPM parameters. For example, under a certain error rate constraint, one can start by first deciding the permutation set with $d_{\min}$ and then $M \geq d_{\min}$ to make sure that that the system diversity is bounded by $d_{\min}N_r$ or kN_r in fast-fading channel or slow-fading channel, respectively.

TABLE 2. Comparison of the SPM diversity in fast-fading channel and the slow-fading channel, i.e., $d_{\min}$ and k. For a given transmitted $(\mathbf{p}, s)$, we select the error pair with $\tilde{s} = s$ and $\tilde{\mathbf{p}}$ with minimum Hamming distance $d_{\min}$. The value of k is obtained by the approximation in (23) and the full connected neural network.

$\mathbf{p}^\top$	$\tilde{\mathbf{p}}^\top$	$d_{\min}$	k
$[1,2,3,4]$	$[1,2,4,3]$	2	1.0
	$[1,3,4,2]$	3	2.0
	$[2,3,4,1]$	4	2.8

Table 2 shows the diversity of the SPM in fast-fading channel and slow-fading channel by using the error pair with $\mathbf{s} = \tilde{\mathbf{s}}$ and the Hamming distance between $(\mathbf{p},\tilde{\mathbf{p}})$ equals the minimum Hamming distance $d_{\min}$. The diversity in slow-fading channel is less than that in fast-fading channel, since the summation of $d_{\min}$ dependent random variables is approximated by a Gamma random variable with shape parameter k (23). In fast-fading channel, these random variables are independent and their summation is exactly a Gamma random variable with shape parameter $d_{\min}$. In other words, signals may experience the same channel fading gain at different time instants in slow-fading channel, resulting in the time dependency that degrades the SPM diversity. Nevertheless, by adding more transmit antennas, this dependency can be reduced and thus the SPM diversity in slow-fading channel can approach to that in fast-fading channel [31]. Compared with SM which is a special case of SPM with $d_{\min} = 1$ and $T = 1$ as mentioned previously, the SM diversity is fixed to N_r. Meanwhile, SPM can flexibly and multiplicatively increase the diversity by $d_{\min}$ or k times to provide different trade-offs between the reliability and throughput.

Note that for the purpose of consistency and comparison, same SPM system model (9) and analysis procedure are adopted for both the slow-fading channel and fast-fading channel. Alternatively, the transmit signal in slow-fading channel can be formulated as a matrix $\mathbf{S} \in \chi^{T\times N_t}$, e.g., with $M = T = 4$ and permutation vector $[1,2,3,4]^\top$, we have

$$\mathbf{S}\left(\begin{bmatrix}1\\2\\3\\4\end{bmatrix}\right) = \begin{bmatrix}s&0&0&0\\0&s&0&0\\0&0&s&0\\0&0&0&s\end{bmatrix}. \tag{36}$$

Based on this formulation, the minimum coding gain distance (CGD) approach can be applied to analyze the transmit diversity [18]. Using the parameters in Table 2 as examples, the diversity of the pair $(\mathbf{p},\tilde{\mathbf{p}}) = ([1,2,3,4]^\top,[1,2,4,3]^\top)$ and $s = \tilde{s}$ equals the number of nonzero eigenvalues of $\mathbf{D}\cdot\mathbf{D}^H$,

where $\mathbf{D}$ is the difference between the transmit symbol matrix with $\mathbf{p}$ and its erroneous symbol matrix with $\tilde{\mathbf{p}}$

$$\mathbf{D}=\mathbf{S}\left(\begin{bmatrix}1\\2\\3\\4\end{bmatrix}\right)-\mathbf{S}\left(\begin{bmatrix}1\\2\\4\\3\end{bmatrix}\right)=\begin{bmatrix}0&0&0&0\\0&0&0&0\\0&0&s&-s\\0&0&-s&s\end{bmatrix}. \quad (37)$$

After some computations, single diversity is reported in this case. The diversities associated with other two erroneous permutation vectors $\tilde{\mathbf{p}}=[1,3,4,2]^\top$ and $\tilde{\mathbf{p}}=[2,3,4,1]^\top$ can be computed as well, which are 2 and 3, respectively. Compared with the value of k learned by the neural network in Table 2, we can see that the proposed analysis approach accurately estimates the diversity as the standard CGD procedure for slow-fading channel, while the error rate analysis result will be validated by numerical simulations later in Sec. VI.

With the unconditional MGF at hand, the PEP can be computed by integration

$$f(\mathbf{s},\mathbf{p}\to\tilde{\mathbf{s}},\tilde{\mathbf{p}})=\frac{1}{2\pi j}\int_{\hat{z}-j\infty}^{\hat{z}+j\infty}M_\Lambda(z)\frac{\mathrm{d}z}{z}, \quad (38)$$

which can be tightly approximated by numerical methods, e.g., saddlepoint approximation [32, eq. (12)]

$$f_{\mathrm{SA}}(\mathbf{s},\mathbf{p}\to\tilde{\mathbf{s}},\tilde{\mathbf{p}})=\frac{1}{\hat{s}\sqrt{2\pi\,\log(M(\hat{z}))''}}e^{\log(M(\hat{z}))}, \quad (39)$$

where $\hat{z}=\frac{1}{2}$ as used in (30). The BER P_b is computed by applying the union bound

$$P_b\le\frac{\sum_{\forall(\mathbf{s},\mathbf{p})}\sum_{\forall(\tilde{\mathbf{s}},\tilde{\mathbf{p}})}d^{(b)}_{\mathbf{s},\mathbf{p},\tilde{\mathbf{s}},\tilde{\mathbf{p}}}f_{\mathrm{SA}}(\mathbf{s},\mathbf{p}\to\tilde{\mathbf{s}},\tilde{\mathbf{p}})}{|\chi|K\log_2(|\chi|K)}, \quad (40)$$

where $d^{(b)}_{\mathbf{s},\mathbf{p},\tilde{\mathbf{s}},\tilde{\mathbf{p}}}$ is the number of different bits between the demapped bits of $(\mathbf{s},\mathbf{p})$ and $(\tilde{\mathbf{s}},\tilde{\mathbf{p}})$. Since the BER analysis involves the computations of all error pairs, the permutation set with same $d_{\min}$ may have different Hamming distance matrix (4), leading to different BERs. Nevertheless, as the error rate is dominated by the minimum Hamming distance $d_{\min}$, such performance differences are generally negligible.

V. STBC-SPM AND QSPM

To show that SPM is highly compatible to other SM/IM techniques, the STBC-SPM and QSPM systems are proposed in this section. In both subsections, we first review STBC-SM and QSM, and then introduce the integration with permutation vectors for better reliability.

A. STBC-SPM

In [18], STBC-SM was proposed to improve the error rate performance of SM by combining with STBC. Specifically, by using the Alamouti code [33],

$$\begin{bmatrix}s_1&-s_2^*\\s_2&s_1^*\end{bmatrix}, \quad (41)$$

four transmitted STBC-SM codewords $\tilde{\mathbf{A}}_i$, $i=1,\ldots,4$ are designed for a MIMO system with $N_\mathrm{t}=4$ by simultaneously activating two transmit antennas during two time instants

$$\tilde{\mathbf{A}}_1(s_1,s_2)=\begin{bmatrix}s_1&-s_2^*\\s_2&s_1^*\\0&0\\0&0\end{bmatrix},\quad \tilde{\mathbf{A}}_2(s_1,s_2)=\begin{bmatrix}0&0\\0&0\\s_1&-s_2^*\\s_2&s_1^*\end{bmatrix},$$
$$\tilde{\mathbf{A}}_3(s_1,s_2)=\begin{bmatrix}0&0\\s_1&-s_2^*\\s_2&s_1^*\\0&0\end{bmatrix}e^{j\theta_1},\quad \tilde{\mathbf{A}}_4(s_1,s_2)=\begin{bmatrix}s_2&s_1^*\\0&0\\0&0\\s_1&-s_2^*\end{bmatrix}e^{j\theta_1}, \quad (42)$$

where the rotation angle θ_1 depends on the modulation alphabet and is used to maximize the coding gain and diversity [18]. For each transmission, STBC-SM transmits two QAM symbols (s_1,s_2) and additional two bits by using the indices of the selected codewords $\tilde{\mathbf{A}}_i$. For instance, bits '00' and '01' are modulated by selecting the codedwords $\tilde{\mathbf{A}}_1$ and $\tilde{\mathbf{A}}_2$, respectively.

For the proposed STBC-SPM, since the permutation in SPM is used to disperse the spatial symbols in time coordinate, the STBC-SPM further increases the transmission period T times larger than that of STBC-SM. Specifically, the data bits are first used to select a permutation vector from the set $C_{N_\mathrm{t},T}(K,d_{\min})$. Entries in the adopted permutation vector are then used as the *codeword indices* to cascade the codewords in (42), forming an STBC-SPM codeword. Taking $T=2$ as an example, an STBC-SPM codeword is constituted by two STBC-SM codewords $\tilde{\mathbf{A}}_i$ and $\tilde{\mathbf{A}}_j$

$$\mathbf{A}(s_1,s_2,s_3,s_4)=\left[\,\tilde{\mathbf{A}}_i(s_1,s_2)\;\tilde{\mathbf{A}}_{j,j\neq i}(s_3,s_4)\,\right], \quad (43)$$

where each codeword conveys different QAM symbols. In fact, for STBC-SM with $N_\mathrm{t}=4$, we have another two codewords in addition to those in (42)

$$\tilde{\mathbf{A}}_5(s_1,s_2)=\begin{bmatrix}s_1&-s_2^*\\0&0\\s_2&s_1^*\\0&0\end{bmatrix}e^{j\theta_2},\quad \tilde{\mathbf{A}}_6(s_1,s_2)=\begin{bmatrix}0&0\\s_1&-s_2^*\\0&0\\s_2&s_1^*\end{bmatrix}e^{j\theta_2}, \quad (44)$$

where θ_2 is another rotation angle imposed for performance optimization. The codewords multiplied by the same rotation angles are orthogonal to each other, i.e., $(\tilde{\mathbf{A}}_1,\tilde{\mathbf{A}}_2)$, $(\tilde{\mathbf{A}}_3,\tilde{\mathbf{A}}_4)$, and $(\tilde{\mathbf{A}}_5,\tilde{\mathbf{A}}_6)$. Since two bits are transmitted by either using 4 or 6 codewords, $\tilde{\mathbf{A}}_5$ and $\tilde{\mathbf{A}}_6$ are generally ignored in the STBC-SM system. Nevertheless, STBC-SPM benefits from these two codewords. Following the example that cascades two STBC-SM codewords, STBC-SPM can only use $4\cdot 3=12$ combinations, indicating that three bits are transmitted. The number of codeword combinations increases to $6{\cdot}5=30$ when 6 codewords are used. This means that, one can select 16 combinations to transmit 4 bits. In this case, the throughputs of the spatial symbol of STBC-SM and STBC-SPM are identical, i.e., 1 bps/Hz, while STBC-SPM

achieves lower error rate due to the permutation that further exploits the diversity.

Like STBC-SM applying the rotation angles to codewords to maximize the coding gain and diversity, we split the permutation vectors into groups and impose different rotation angles on the transmitted codewords when different groups of the permutation vectors are adopted. In this way, the minimum Hamming distance of the permutation set can be maximized by rotation. For example, when two STBC-SM codewords are cascaded, we can group the permutation vectors as follows

$$\begin{aligned}\mathcal{P}_1 &= \left\{\begin{bmatrix}6\\1\end{bmatrix},\begin{bmatrix}1\\4\end{bmatrix},\begin{bmatrix}2\\5\end{bmatrix},\begin{bmatrix}3\\6\end{bmatrix}\right\},\\ \mathcal{P}_2 &= \left\{\begin{bmatrix}4\\1\end{bmatrix},\begin{bmatrix}5\\2\end{bmatrix},\begin{bmatrix}6\\3\end{bmatrix},\begin{bmatrix}1\\6\end{bmatrix}\right\},\\ \mathcal{P}_3 &= \left\{\begin{bmatrix}2\\1\end{bmatrix},\begin{bmatrix}3\\2\end{bmatrix},\begin{bmatrix}5\\4\end{bmatrix},\begin{bmatrix}6\\5\end{bmatrix}\right\},\\ \mathcal{P}_4 &= \left\{\begin{bmatrix}1\\2\end{bmatrix},\begin{bmatrix}2\\3\end{bmatrix},\begin{bmatrix}4\\5\end{bmatrix},\begin{bmatrix}5\\6\end{bmatrix}\right\},\end{aligned} \tag{45}$$

where the Hamming distance $d(\mathbf{p}_a, \mathbf{p}_b) = 2$ for the permutation vectors in the same group $\mathbf{p}_a, \mathbf{p}_b \in \mathcal{P}_i$, while we have $d(\mathbf{p}_a, \mathbf{p}_b) \leq 2$ for the permutation vectors in different groups $\mathbf{p}_a \in \mathcal{P}_i$ and $\mathbf{p}_b \in \mathcal{P}_j$ with $i \neq j$. Then, depending on the group index i, in additional to θ_i in (42) and (44), another rotation angle

$$\phi_i = \frac{(i-1)\pi}{8} \tag{46}$$

is imposed on the codewords using QSPK and 16QAM modulations as stated in [18]. Following (43), the transmitted codeword of STBC-SPM is given by

$$\mathbf{A}(s_1, s_2, s_3, s_4) = \left[\tilde{\mathbf{A}}_{p_{k,1}}(s_1, s_2)e^{j\phi_i}\ \tilde{\mathbf{A}}_{p_{k,2}}(s_3, s_4)e^{j\phi_i}\right] \tag{47}$$

with $\mathbf{p}_k \in \mathcal{P}_i$ and $p_{k,j} = 1, \ldots, 6$.

The extension from STBC-SM to STBC-SPM can be applied to other advanced SM techniques such as DT-SM [34], [35]. In particular, the transmit signal of DT-SM includes the double space-time transmit diversity (DSTTD) codeword [36] and the spatial constellation (SC) codeword [37], [38]. Since up to $16\binom{N_t}{N_t-4}$ SC codewords can be generated and 4 QAM symbols are conveyed by the DSTTD codeword, the DT-SM system achieves higher spectral efficiency compared with other SM systems. By utilizing the permutation vectors to cascade the DT-SM codewords and conduct in-depth performance analysis, one can design the DT-SPM that further elevates the transmission reliability.

B. QSPM

Since SM transmits one QAM symbol at a time with the spatial symbol whose number of bits is logarithmically proportional to the transmit antenna number, SM has lower spectral efficiency than the spatial multiplexing technique. By expanding the spatial symbol into the in-phase and quadrature components, QSM is proposed to enhance the SM throughput [21]. Specifically, compared with SM, the QSM transmitter comprises an additional spatial demultiplexer which assigns the real and imaginary parts of the QAM symbol to various transmit antennas. Thus, we can have two sets of $\lfloor \log_2 N_t \rfloor$ bits to select the active antennas. The transmission model of QSM takes the form of:

$$\mathbf{y} = \mathbf{h}_{q_\Re} s_\Re + j\mathbf{h}_{q_\Im} s_\Im + \mathbf{n}, \tag{48}$$

where $s_\Re$ and $s_\Im$ are the real and imaginary parts of the QAM symbol, respectively. The two indices $q_\Re$ and $q_\Im$ are the in-phase and quadrature spatial symbols, respectively, which are used to indicate the active antenna for the transmission of $s_\Re$ and $s_\Im$. For example, given $(q_\Re, q_\Im) = (2, 4)$ and $s = (1 + 3j)/\sqrt{10}$, the transmit signal is represented as $[0, 1/\sqrt{10}, 0, 3j/\sqrt{10}]^\top$. Although multiple transmit antennas are activated, the interference between signals from different transmit antennas is avoided. This is because that, the real part and imaginary part of the QAM symbol are orthogonal to each other due to the cosine and sine carriers.

By integrating the permutation vectors with QSM, we propose the QSPM with the system model based on (9) and (48):

$$\mathbf{Y} = \mathbf{H}(\mathbf{p}_\Re)\mathrm{diag}(\mathbf{s}_\Re) + \mathbf{H}(\mathbf{p}_\Im)\mathrm{diag}(\mathbf{s}_\Im) + \mathbf{V}, \tag{49}$$

where $\mathbf{s}_\Re$ and $\mathbf{s}_\Im$ are the real part and imaginary part of the vector $\mathbf{s}$ defined in (8) which may comprise same or different QAM symbols depending on the parameter M. The permutation vector $\mathbf{p}_\Re$ is used to activate various transmit antennas at successive time instants for the transmission of $\mathbf{s}_\Re$. Likewise, $\mathbf{p}_\Im$ controls the active transmit antennas to successively transmit the imaginary part signal $\mathbf{s}_\Im$. In this way, the signals are dispersed along the time coordinate and the diversity gains are achieved. With this setting, the number of bits transmitted by QSPM is $2\lfloor \log_2 K \rfloor + \frac{T}{M}\log_2 |\chi|$.

Alternatively, one can apply the permutation vector to jointly select the active transmit antennas for the real and imaginary parts transmissions at the same time instant. In other words, the permutation vector includes $q_\Re$ and $q_\Im$ in (48). For example, the permutation vector $[1, 4]^\top$ indicates that the first antenna is activated to transmit the real part of the QAM symbol, and the fourth antenna is used for the transmission of the imaginary part. Compared with the system in (49), the latency can be reduced to half. However, like SPM in slow-fading channel, when two elements of the permutation vector are used at each time instant, the diversity may be lower than that of (49). Therefore, in the following simulations, we still adopt the system model in (49) for our QSPM simulation.

VI. SIMULATION RESULTS

In this section, we first validate our theoretical analysis results and then demonstrate the superior performances of SPM and STBC-SPM by means of Monte Carlos simulations. The optimal ML decoder is adopted at the receiver side for all the simulations and analyses.

The numerical and analytical BER comparisons of SPM are depicted in Fig. 2 for various minimum Hamming distances $d_{\min}$ and QAM modulations with $(N_t, N_r, T, M) = (4, 1, 4, 4)$. Both the slow-fading channel and fast-fading

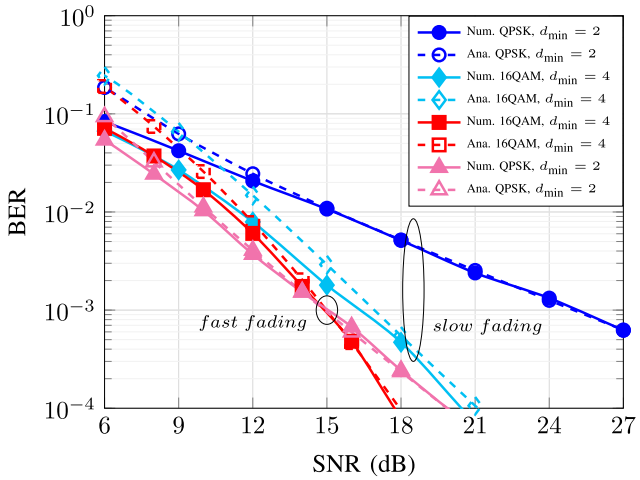

FIGURE 2. Comparison of the numerical and analytical BERs of SPM with $(N_t, N_r, T, M) = (4, 1, 4, 4)$. Both the slow-fading channel and fast-fading channel are considered.

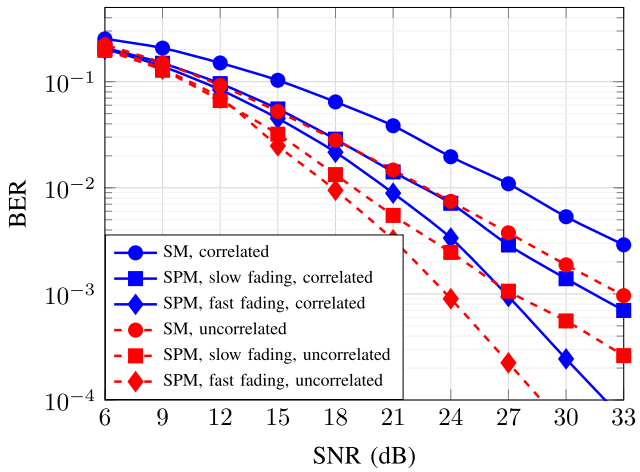

FIGURE 3. BER comparisons of the SM-MIMO and SPM-MIMO systems with $(N_t, N_r) = (4, 1)$ in slow-fading channel and fast fading channel, under 3 bps/Hz rate constraint. Both the channels with and without spatial correlation are considered.

channel are considered. The solid lines represent the empirical results, while the dashed lines denote theoretical analyses. The tight overlaps between the analytical and numerical BERs confirm the accuracy of our analyses for different transmission parameters and fading channels. We simulated two systems with $(|\chi|, d_{\min})$ being (16, 4) and (4, 2), respectively. Since $M = 4$, the system diversity is bounded by $d_{\min}$ as discussed in Section IV. Therefore, Although the former adopts higher modulation (16QAM), its larger diversity leads to better error rate improvement as SNR increases.

Fig. 3 aims at comparing the performances of SM and SPM in different fading channels with $(N_t, N_r = (4, 1)$. Note that the SM system yields the same error rate performance in either slow-fading channel or fast-fading channel due to the transmission of the single time instant. The SM system adopts BPSK modulation so that its throughput is 3 bps/Hz. The SPM parameters are $(T, M, d_{\min}, K) = (2, 2, 2, 4)$ and 16QAM modulation, resulting in throughput 3 bps/Hz as well. Both the channels with and without spatial correlations are considered. For the uncorrelated channel with target BER 10^{-3}, the SPM system in slow-fading channel and fast-fading channel achieve 6 and 12 dB SNR gains over the SM system, respectively.

For the correlated channels, the exponential correlation matrix model is adopted [18]

$$\mathbf{H}_{sc} = \mathbf{R}_T^{1/2}\mathbf{H}\mathbf{R}_R^{1/2}, \tag{50}$$

where $\mathbf{R}_T^{1/2} \in \mathbb{C}^{N_t \times N_t}$ and $\mathbf{R}_R^{1/2} \in \mathbb{C}^{N_r \times N_r}$ with $R_{Ti,j} = R_{Ri,j} = \rho^{-|i-j|}$ are the correlation matrices used to model the correlation at the transmitter and receiver sides, respectively. We set $\rho = 0.9$ to simulate the highly-correlated scenario where SM fails to achieve BER 10^{-3} even at high SNR. Nevertheless, SPM in slow-fading channel and fast-fading channel can provide this error rate performance at around 32 dB and 27 dB, respectively.

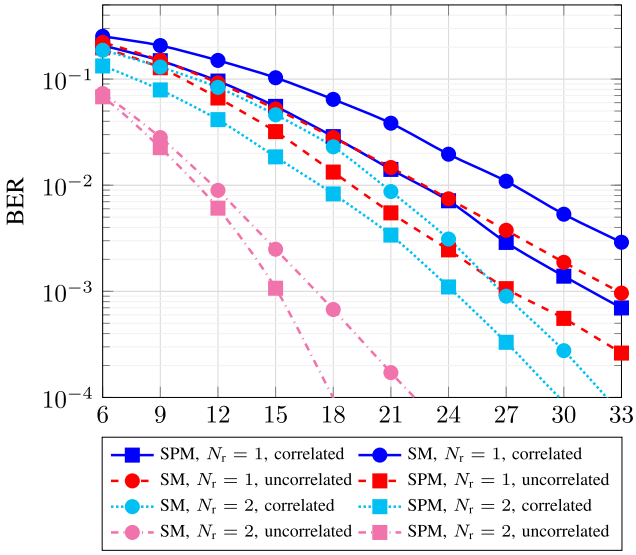

FIGURE 4. BER comparisons of the SPM-MIMO system in slow-fading channel and SM-MIMO system with and without spatial correlation, under 3 bps/Hz rate constraint. $N_t = 4$ and both $N_r = 1$ and $N_r = 2$ are considered.

Fig. 4 compares SM and SPM in slow-fading channel with $N_t = 4$ and different numbers of receive antennas. We see that for all the scenarios, i.e., $N_r = 1$ and 2; spatially-uncorrelated and spatially-correlated channels. SPM shows better error performance than SM. Note that this channel is assumed to be slow-fading, which can be regarded as a performance *lower bound* since in many cases, the time correlation of the channel fading gains is smaller and thus less time dependency that degrades the SPM performance.

While previous simulations focus on the severe environments where only 3 bps/Hz can be supported, Fig. 5 compares SM and SPM with higher throughputs. We increase the number of transmit antennas to 6 to allow systems operating with higher throughputs. With more transmit antennas, SM can activate the antennas with less correlations e.g., first and sixth antennas, and SPM can utilize more permutation vectors.

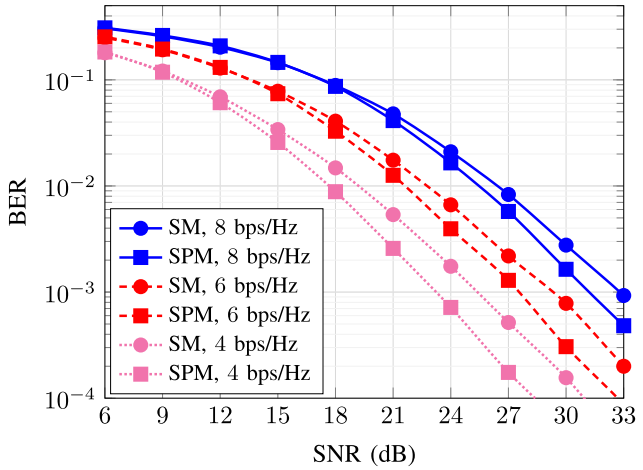

FIGURE 5. BER comparisons of the SPM-MIMO and SM-MIMO system with $(N_t, N_r) = (6, 2)$ in spatially-correlated fast-fading channel, under various rate constraints.

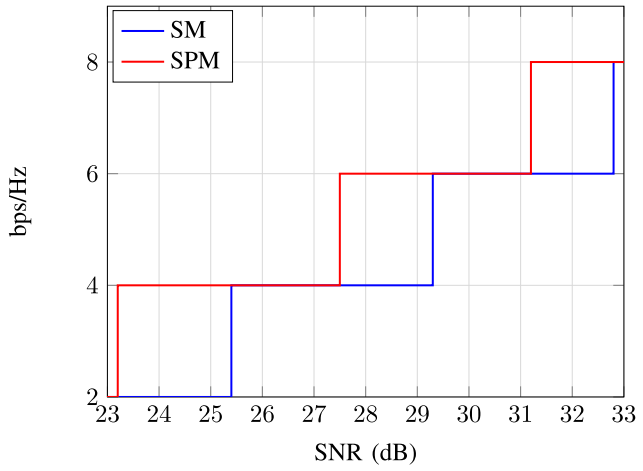

FIGURE 6. Spectral efficiency comparisons of the SPM-MIMO and SM-MIMO system with $(N_t, N_r) = (6, 2)$ in spatially-correlated fast-fading channel, under BER constraint 10^{-3}.

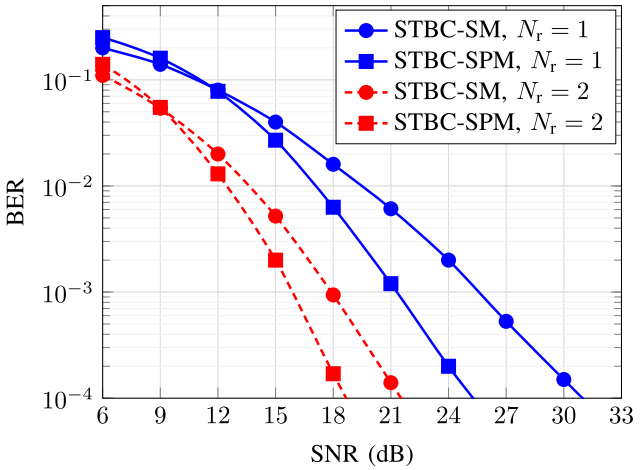

FIGURE 7. BER comparisons of MIMO systems using STBC-SM and STBC-SPM with $N_t = 4$ and various N_r in spatially-correlated channel, under 3 bps/Hz rate constraint.

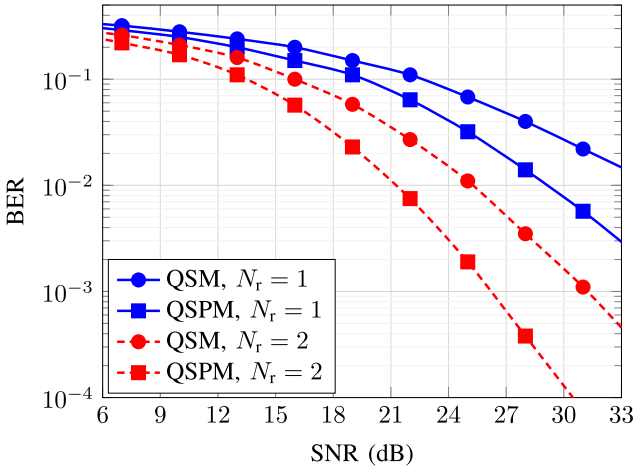

FIGURE 8. BER comparisons of MIMO systems using QSM and QSPM with $N_t = 4$ and various N_r in spatially-correlated channel, under 6 bps/Hz rate constraint.

The numerical results demonstrate that SPM stills provide better error rate performance than SM. Nevertheless, the error rate improvement of SPM decreases when the throughput increases, since SM can be interpreted as a special case of SPM with $T = 1$ such that $(d_{\min}, M) = (1, 1)$ as mentioned previously. The setting of this *special SPM* seeks for the throughput maximization. Therefore, to meet high throughput requirement, the reliability of SPM should be reduced and thus the resulting SPM system becomes more similar to the SM system. Also, when higher QAM modulations are adopted to achieve the high throughputs, the system performance is dominated by the error rate of the QAM symbols, rather than the spatial symbols.

To further compare the performance between SM and SPM, Fig. 6 demonstrates their achievable throughputs with the BER constraint 10^{-3}, under the same environment and parameter settings as the simulation in Fig. 5. With this spectral efficiency comparison, we can see that when spectral efficiency increases from 4 bps/Hz to 8 bps/Hz, the improvement of SPM becomes less significant, i.e., from 2.2 dB to 1.6 dB. The reason is that, as mentioned in Fig. 5, when one adjusts the parameters of SPM to pursue high throughput, the resulting SPM system resembles the SM system. Note that in some cases the maximum throughput of SPM may be larger than that of SM. For example, with $N_T = 7$, SM transmits 2 bits by the spatial symbol at each time instant. However, with $T = 2$, the number of permutation vectors that SPM can utilize is $7 \cdot 6 = 42 > 2^5$, implying that up to 2.5 bits can be transmitted by the spatial symbol per time instant. The reason behind is that, when the number of transmit antennas is not power of two, some of them cannot be used to improve the throughput. With the permutation, the number of usable permutations becomes $\frac{N!}{(N-T)!}$ so that more bits may be transmitted. For the techniques like STBC-SM or DT-SM where the transmit entities used by SM are codewords, since the number of codewords are generally not power of two, this advantage is more pronounced.

Last, Fig. 7 and Fig. 8 show the numerical comparisons of the advanced SM techniques with and without the integration

of SPM, i.e., STBC-SM versus STBC-SPM and QSM versus QSPM, respectively. We set $N_t = 4$ and various N_r. From the numerical results, we discover that compared with the improvement of STBC-SPM (with respect to STBC-SM), the improvement of QSPM (with respect to QSM) is more significant. This is because that, QSM is proposed to provide higher spectral efficiency, while STBC-SM aims at enhancing the reliability of SM, whose design goal is similar to that of SPM. Thus, the combination of QSM and SPM leads to larger enhancement, up to 5 dB SNR gain at BER 10^{-3} and $N_r = 2$. Nevertheless, STBC-SPM still achieves 2 dB improvement at the same setting and BER requirement. The improvement further increases when $N_r = 1$ such that diversity introduced by SPM is essential. Around 5 dB SNR gain is obtained by STBC-SPM compared with STBC-SM. The superior performances of STBC-SPM and QSPM demonstrate that the application of permutation vectors benefits the SM-based MIMO systems.

VII. CONCLUSIONS AND FUTURE WORKS

In this work, we proposed and theoretically analyzed the SPM technique for the MIMO system. By utilizing a permutation vector to sequentially select the transmit antennas or STBC-SM codewords at successive time instants, both SPM and STBC-SPM deliver superior performance. The theoretical analyses established the BER model and explained the reason why SPM performs better in fast-fading channel than in slow-fading channel by calculating the diversity. Numerical simulations demonstrate that SPM provides transmit diversity and thus can operate in the severe environments like low receive diversity or spatially-correlated channels.

We hope that the framework of SPM reported here serves as a starting point for future research that exploits the permutations to the SM/IM systems. Several interesting research directions are as follows: First, the concept of imposing rotation angles on the transmit data corresponding to different permutation vectors can be directly applied to SPM so as to improve the diversity and coding gains. Advanced coding technique can be applied for the transmitted QAM symbols as mentioned in Section III. Second, when multiple active transmit antennas are allowed, i.e., GSM [19], [20], the generalized spatial permutation modulation (GSPM) can be expected to further enhance the transmission efficiency. At the receiver side, a low-complexity SPM detector is another practical research topic like our previous work [30], which is omitted here. The theoretical analyses of the spectral efficiency of SPM and other permutation-based SM systems like QSPM and STBC-SPM are also of interest. Last but not least, the permutation can be easily extended and applied to other IM techniques. For example, the IM-OFDM system partitions the subcarriers into small groups where only one subcarrier is used for transmission [11], [12]. By using the permutation vectors to select the subcarrier indices for various groups, we have the index permutation modulation (IPM)-OFDM system that disperses the signals in the frequency coordinate to gain the diversity.

REFERENCES

[1] V. Tarokh, N. Seshadri, and A. R. Calderbank, "Space-time codes for high data rate wireless communication: Performance criterion and code construction," *IEEE Trans. Inf. Theory*, vol. 44, no. 2, pp. 744–765, Mar. 1998.

[2] T.-D. Chiueh, P.-Y. Tsai, and I.-W. Lai, *Baseband Receiver Design for Wireless MIMO–OFDM Communications*, 2nd ed. Hoboken, NJ, USA: Wiley, 2012.

[3] R. Y. Mesleh, H. Haas, and S. Sinaovic, C. W. Ahn, and S. Yun, "Spatial modulation," *IEEE Trans. Veh. Technol.*, vol. 57, no. 4, pp. 2228–2241, Jul. 2008.

[4] E. Başar, M. Wen, R. Mesleh, M. D. Renzo, Y. Xiao, and H. Haas, "Index modulation techniques for next-generation wireless networks," *IEEE Access*, vol. 5, pp. 16693–16746, Aug. 2017.

[5] S. Sugiura, T. Ishihara, and M. Nakao, "State-of-the-art design of index modulation in the space, time, and frequency domains: Benefits and fundamental limitations," *IEEE Access*, vol. 5, pp. 21774–21790, Oct. 2017.

[6] S. Althunibat and R. Mesleh, "Enhancing spatial modulation system performance through signal space diversity," *IEEE Commun. Lett.*, vol. 22, no. 6, pp. 1136–1139, Jun. 2018.

[7] M. Di Renzo, H. Haas, A. Ghrayeb, S. Sugiura, and L. Hanzo, "Spatial modulation for generalized MIMO: Challenges, opportunities, and implementation," *Proc. IEEE*, vol. 102, no. 1, pp. 56–103, Jan. 2014.

[8] M. Di Renzo and H. Haas, "Bit error probability of SM-MIMO over generalized fading channels," *IEEE Trans. Veh. Technol.*, vol. 61, no. 3, pp. 1124–1144, Mar. 2012.

[9] P. Yang, Y. L. Guan, Y. Xiao, M. Di Renzo, S. Li, and L. Hanzo, "Transmit precoded spatial modulation: Maximizing the minimum Euclidean distance versus minimizing the bit error ratio," *IEEE Trans. Wireless Commun.*, vol. 15, no. 3, pp. 2054–2068, Mar. 2016.

[10] H. Haas and S. Dimitrov, *Principles of LED Light Communications*. Cambridge, U.K.: Cambridge Univ. Press, 2015.

[11] E. Başar, Ü. Aygölü, E. Panayırcı, and H. V. Poor, "Orthogonal frequency division multiplexing with index modulation," *IEEE Signal Process. Lett.*, vol. 61, no. 22, pp. 5536–5549, Nov. 2013.

[12] T. Mao, Z. Wang, Q. Wang, S. Chen, and L. Hanzo, "Dual-mode index modulation aided OFDM," *IEEE Access*, vol. 5, pp. 50–60, 2016.

[13] Y. Bian, X. Cheng, M. Wen, L. Yang, H. V. Poor, and B. Jiao, "Differential spatial modulation," *IEEE Trans. Veh. Technol.*, vol. 64, no. 7, Jul. 2015.

[14] S. Sugiura, S. Chen, and L. Hanzo, "Coherent and differential space-time shift keying: A dispersion matrix approach," *IEEE Trans. Commun.*, vol. 58, no. 11, pp. 3219–3230, Nov. 2010.

[15] S. Sugiura, S. Chen, and L. Hanzo, "Generalized space-time shift keying designed for flexible diversity-, multiplexing- and complexity-tradeoffs," *IEEE Trans. Wireless Commun.*, vol. 10, no. 4, pp. 1144–1153, Apr. 2011.

[16] S. Sugiura, S. Chen, and L. Hanzo, "A universal space-time architecture for multiple-antenna aided systems," *IEEE Commun. Surveys Tuts.*, vol. 14, no. 2, pp. 401–420, Jan. 2012.

[17] I. A. Hemadeh, M. El-Hajjar, S. Won, and L. Hanzo, "Multi-set space-time shift-keying with reduced detection complexity," *IEEE Access*, vol. 4, pp. 4234–4246, 2016.

[18] E. Başar, Ü. Aygölü, E. Panayırcı, and H. V. Poor, "Space-time block coded spatial modulation," *IEEE Trans. Commun.*, vol. 59, no. 3, pp. 823–832, Mar. 2011.

[19] A. Younis, N. Serafimovski, R. Mesleh, and H. Haas, "Generalised spatial modulation," in *Proc. Conf. Rec. Forty Fourth Asilomar Conf. Signals, Syst. Comput.*, Nov. 2010, pp. 1498–1502.

[20] T. L. Narasimhan, P. Raviteja, and A. Chockalingam, "Generalized spatial modulation in large-scale multiuser MIMO systems," *IEEE Trans. Wireless Commun.*, vol. 14, no. 7, pp. 3764–3779, Jul. 2015.

[21] R. Mesleh, S. S. Ikki, and H. M. Aggoune, "Quadrature spatial modulation," *IEEE Trans. Veh. Technol.*, vol. 64, no. 6, pp. 2738–2742, Jun. 2015.

[22] I.-W. Lai, J.-M. Wang, J.-W. Shih, and T. Chiueh, "Adaptive MIMO detector using reduced search space and its error rate estimator in ultra dense network," *IEEE Access*, vol. 7, pp. 6774–6781, Dec. 2018.

[23] N. L. Biggs, *Discrete Mathematics*, 2nd ed. London, U.K.: Oxford Univ. Press, 2003.

[24] E. Biglieri and M. Elia, "Optimum permutation modulation codes and their asymptotic performance," *IEEE Trans. Inf. Theory*, vol. 22, no. 6, pp. 751–753, Nov. 1976.

[25] I. W. Lai, C. H. Lee, K. C. Chen, and E. Biglieri, "Path-permutation codes for end-to-end transmission in ad hoc cognitive radio networks," *IEEE Trans. Wireless Commun.*, vol. 14, no. 6, pp. 3309–3321, Jun. 2015.

[26] H. C. Ferreira, A. J. H. Vinck, T. G. Swart, and I. de Beer, "Permutation trellis codes," *IEEE Trans. Commun.*, vol. 53, no. 11, pp. 1782–1789, Nov. 2005.
[27] N. Ishikawa, S. Sugiura, and L. Hanzo, "50 years of permutation, spatial and index modulation: From classic RF to visible light communications and data storage," *IEEE Commun. Surveys Tuts.*, vol. 20, no. 3, pp. 1905–1938, 3rd Quart., 2018.
[28] A. Younis, S. Sinanovic, M. Di Renzo, R. Mesleh, and H. Haas, "Generalised sphere decoding for spatial modulation," *IEEE Trans. Commun.*, vol. 61, no. 7, pp. 2805–2815, Jul. 2013.
[29] R. Rajashekar, K. V. S. Hari, and L. Hanzo, "Reduced-complexity ML detection and capacity-optimized training for spatial modulation systems," *IEEE Trans. Commun.*, vol. 62, no. 1, pp. 112–125, Jan. 2014.
[30] J.-C. Chi, Y.-C. Yeh, I.-W. Lai, and Y.-H. Huang, "Sphere decoding for spatial permutation modulation MIMO systems," in *Proc. IEEE Int. Conf. Commun. (ICC)*, May 2017, pp. 1–6.
[31] J.-W. Shih, J.-C. Chi, Y.-H. Huang, P.-Y. Tsai, and I.-W. Lai, "Theoretical performance analysis assisted by machine learning for spatial permutation modulation (SPM) in slow-fading channels," in *Proc. IEEE Int. Conf. Commun. (ICC)*, May 2018, pp. 1–6.
[32] A. Martinez and A. G. I. Fàbregas, and G. Caire, "Error probability analysis of bit-interleaved coded modulation," *IEEE Trans. Inf. Theory*, vol. 52, no. 1, pp. 262–271, Jan. 2006.
[33] S. Alamouti, "A simple transmit diversity technique for wireless communications," *IEEE J. Sel. Areas Commun.*, vol. 16, no. 8, pp. 1451–1458, Oct. 1998.
[34] M.-T. Le, V.-D. Ngo, H.-A. Mai, X. N. Tran, and M. Di Renzo, "Spatially modulated orthogonal space-time block codes with non-vanishing determinants," *IEEE Trans. Commun.*, vol. 62, no. 1, pp. 85–99, Jan. 2014.
[35] M.-T. Le, T.-D. Nguyen, X.-N. Tran, and V.-D. Ngo, "On the combination of double space time transmit diversity with spatial modulation," *IEEE Trans. Wireless Commun.*, vol. 17, no. 1, pp. 170–181, Jan. 2018.
[36] J. Wu, Y. R. Zheng, A. Gumaste, and C. Xiao, "Error performance of double space time transmit diversity system," *IEEE Trans. Wireless Commun.*, vol. 6, no. 9, pp. 3191–3196, Sep. 2007.
[37] T. P. Nguyen, M. T. Le, V. D. Ngo, X. N. Tran, and H. W. Choi, "Spatial modulation for high-rate transmission systems," in *Proc. IEEE 79th Veh. Technol. Conf. (VTC Spring)*, May 2014, pp. 1–5.
[38] B. T. Vo, H. H. Nguyen, and N. Quoc-Tuan, "High-rate space–time block coded spatial modulation," in *Proc. IEEE Adv. Technol. Commun.*, Oct. 2015, pp. 1–5.

I-WEI LAI (M'11) received the Ph.D. degree in electrical engineering from the Graduate Institute of Electronics Engineering (GIEE), National Taiwan University, in 2011. He was with RWTH Aachen University, Germany, and Academia Sinica, Taiwan. Since 2017, he has been with the Department of Electrical Engineering, National Taiwan Normal University, as an Assistant Professor. His research interests include signal processing, optimization, and performance analysis for wireless communication networks. He was a recipient of the NTU-GIEE Best Thesis Award, in 2011 for his Ph.D. thesis and is a member of the Phi Tau Phi Scholastic Honor Society. He was recognized as the Exemplary Reviewer of the IEEE TRANSACTIONS ON COMMUNICATIONS, in 2014.

JHIH-WEI SHIH received the B.S. degree in electronic engineering from National Chang Gung University, Taoyuan, Taiwan, in 2016. He is currently pursuing the M.S. degree in electrical engineering with National Taiwan Normal University, Taipei, Taiwan. His research interests include MIMO communication, spatial modulation, and optimization and performance analysis for wireless communication networks.

CHE-WEI LEE received the B.S. degree in electronic engineering from Chang Gung University, Taoyuan, Taiwan, in 2018. He is currently pursuing the degree in electrical engineering with National Taiwan Normal University, Taipei, Taiwan. His research interests include MIMO communication, spatial modulation, and optimization for wireless communication systems.

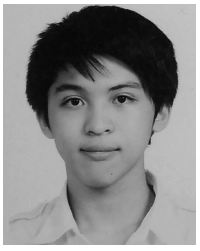

HSU-HSUAN TU received the B.S. degree in electronic engineering from Chang Gung University, Taoyuan, Taiwan, in 2018. He is currently pursuing the M.S. degree in electrical engineering with National Taiwan Normal University, Taipei, Taiwan. His research interests include MIMO communication, spatial modulation, ad hoc cognitive radio networks, and optimization and performance analysis for wireless communication networks.

JUNG-CHUN CHI (S'17) was born in Taiwan, in 1992. He received the B.S. degree in communication engineering from Yuan Ze Univerity, Taoyuan, Taiwan, in 2014, and the M.S. degree from National Tsing Hua University, Hsinchu, Taiwan, in 2016, where he is currently pursuing the Ph.D. degree. His research interests include spatial modulation and VLSI design for communication systems.

JYUN-SIAN WU is currently pursuing the B.S. degree in electrical engineering with National Taiwan Normal University, Taipei, Taiwan. His research interests include MIMO communication, spatial modulation, and low complexity detection for wireless communication systems.

YUAN-HAO HUANG (S'98–M'02) was born in Taiwan, in 1973. He received the B.S. and Ph.D. degrees in electrical engineering from National Taiwan University, Taipei, Taiwan, in 1995 and 2001, respectively. He was a member of the technical staff with VXIS Technology Corporation, from 2001 to 2005. Since 2005, he has been with the Department of Electrical Engineering and the Institute of Communications Engineering, National Tsing Hua University, Taiwan, where he is currently a Professor. His research interests include VLSI design for digital signal processing and telecommunication systems, and biomedical signal processing. He is currently a member of the Advisory Board of Design and Implementation of Signal Processing Systems (DiSPS) Technical Committee of the IEEE Signal Processing Society. He is also a member of VLSI Systems and Applications (VSA) and Giga and Nano Systems (GN) technical committees of the IEEE Circuits and Systems Society. He has also been with the Seasonal School Subcommittee of Membership Board of the IEEE Signal Processing Society, since 2016. He has been an Associate Editor of the *IEEE Signal Processing Magazine*, since 2019.